small NANO MICRO

Tissue engineering

Interface-Directed Self-Assembly of Cell-Laden Microgels

*Behnam Zamanian, Mahdokht Masaeli, Jason W. Nichol, Masoud Khabiry, Matthew J. Hancock, Hojae Bae, and Ali Khademhosseini**

Cell-laden hydrogels show great promise for creating engineered tissues. However, a major shortcoming with these systems has been the inability to fabricate structures with controlled micrometer-scale features on a biologically relevant length scale. In this Full Paper, a rapid method is demonstrated for creating centimeter-scale, cell-laden hydrogels through the assembly of shape-controlled microgels or a liquid–air interface. Cell-laden microgels of specific shapes are randomly placed on the surface of a high-density, hydrophobic solution, induced to aggregate and then crosslinked into macroscale tissue-like structures. The resulting assemblies are cell-laden hydrogel sheets consisting of tightly packed, ordered microgel units. In addition, a hierarchical approach creates complex multigel building blocks, which are then assembled into tissues with precise spatial control over the cell distribution. The results demonstrate that forces at an air–liquid interface can be used to self-assemble spatially controllable, cocultured tissue-like structures.

Keywords:
- cell encapsulation
- microgels
- self-assembly
- tissue engineering

1. Introduction

Organ failure is one of the major causes of death worldwide.[1] However, the number of people who need organ transplants is significantly higher than the number of available organs suitable for transplantation.[1] As a result, the fabrication of three-dimensional (3D) organs is of great importance for regenerative medicine.[2] Recent results have demonstrated the importance of tissue microarchitecture on the resulting function of engineered tissue constructs.[3] Therefore, devising new biomimetic techniques for generating engineered tissues with micrometer-scale resolution is of great scientific interest.

Microfabrication technologies have been applied to cell-culture techniques in an effort to better direct tissue formation and function.[4] As cell–cell and cell–extracellular matrix (ECM) interactions play critical roles in cell and tissue

[*] Prof. A. Khademhosseini
Partners Research Building
Room 252, 65 Landsdowne Street, Cambridge, MA 02139 (USA)
E-mail: alik@rics.bwh.harvard.edu

B. Zamanian,† M. Masaeli,† Dr. J. W. Nichol, M. Khabiry, Dr. M. J. Hancock, Dr. H. Bae, Prof. A. Khademhosseini
Center for Biomedical Engineering
Department of Medicine
Brigham and Women's Hospital
Harvard Medical School
65 Landsdowne Street, Cambridge, MA 02139 (USA)

B. Zamanian, M. Masaeli, Dr. J. W. Nichol, M. Khabiry, Dr. M. J. Hancock, Dr. H. Bae, Prof. A. Khademhosseini
Harvard-MIT Division of Health Sciences and Technology
Massachusetts Institute of Technology
Cambridge, MA 02139 (USA)

M. Masaeli
Department of Electrical and Computer Engineering
Northeastern University
Boston, MA 02115 (USA)

† These authors contributed equally to this work.

‡ B.Z. and M.M. contributed equally to this work. B.Z., M.M., and A.K. conceived of the project and designed methodology and the experiments. B.Z., M.M., and H.B. performed the experiments and the immunostaining. B.Z., M.M., and M.K. analyzed the data. B.Z., M.M., J.N., and A.K. wrote the manuscript; M.J.H. wrote the theoretical rationale. All authors revised the manuscript and consented to the contents of the final version.

DOI: 10.1002/smll.200902326

function, control over the cellular microenvironment could be key to fabricating biomimetic tissue structures.[4] The tissue microarchitecture in the human body is often made of repeating functional units, such as the repeating hexagonal lobules in the liver.[5] As a result, self-assembly of micrometer-scale tissues that is recreate the native microarchitecture of natural tissues is a promising approach for the fabrication of functional tissue constructs.

Self-assembly at various length scales has been previously used for creating complex structures.[6,7] For example, self-assembly has been used at the molecular scale to synthesize biomaterials and at the mesoscale to generate structures both in 2D arrays and 3D mesostructures. Cellular assembly has also been used to create complex tissue structures such as rods, tori, honeycombs,[8,9] knee cartilage,[10] and capillary-filtration devices.[11] We have previously demonstrated the self-assembly of cell-laden microgels by immersion of hydrophilic cell-laden hydrogels into hydrophobic solutions.[7] Higher-order structures were created in predictable patterns and dimensions through control over hydrophilic microgel aggregation and subsequent secondary polymerization. We also demonstrated that microgel dimensions and geometry (i.e., lock-and-key shapes) could direct the assembly of to ordered cocultured constructs. Overall, many positive characteristics and features of self-assembly techniques have been demonstrated. However, major limitations still exist regarding the achievable sizes, shapes, and organization of the resulting fabricated structures.

The encapsulation of cells within cell-laden microgels is an attractive approach for engineered tissue formation.[12,13] In particular, microgels provide control over the cell–cell and cell–ECM contacts found within the cellular microenvironment that can to improve the resulting cellular organization and function.[14] Furthermore, since each microgel can be fabricated with unique properties, it is possible to engineer tissues with multiple chemical microenvironments. In addition, the encapsulation of different growth factors, drugs, or other deliverable molecules in separate blocks is achievable.[14] Photolithography enables building blocks to be engineered with tunable microarchitectures to control the cellular microenvironment, while self-assembly techniques can somewhat control the macroscale environment of the resulting engineered tissues.[7]

In this Full Paper, we describe a technique for the self-assembly of cell-laden microgels on the interface of air and hydrophobic solutions to fabricate 3D tissue constructs with controllable micrometer-scale features. This self-assembly process is guided by the surface-tension forces at the liquid–air interface[6,15] of high-density, hydrophobic solutions. The high-density solution forces the lower-density hydrophilic hydrogels to remain on the surface, similar to techniques previously reported for inorganic materials.[6,16] Hydrophilic, cell-laden hydrogels were randomly placed on the surface of high-density, hydrophobic solutions. Surface tension drove the microgels toward each other to create tissue-like structures through aggregation.[15] These basic thermodynamic mechanisms enabled the fabrication of centimeter-scale tissue structures from cell-laden micrometer-scale hydrogels. The ability to create tissues with these length scales and a clinically relevant overall size suggests that this technique may be beneficial for tissue-engineering applications.

2. Results and Discussion

In this study, we fabricated centimeter-scale tissues from microgel building blocks by using a directed self-assembly approach that utilizes the air–liquid interface. We also demonstrated that a modified version of this process can be used to create centimeter-scale tissues with spatially controlled 3D cocultures. The resulting tissue constructs have micrometer-scale features combined with clinically relevant length scales suggesting potential use for tissue repair and regeneration.

2.1 Self-Assembly Process

Poly(ethylene glycol) dimethacrylate (PEG) hydrogel building blocks of specified geometry and dimensions were created as described (Figure 1A–C) and randomly placed on the

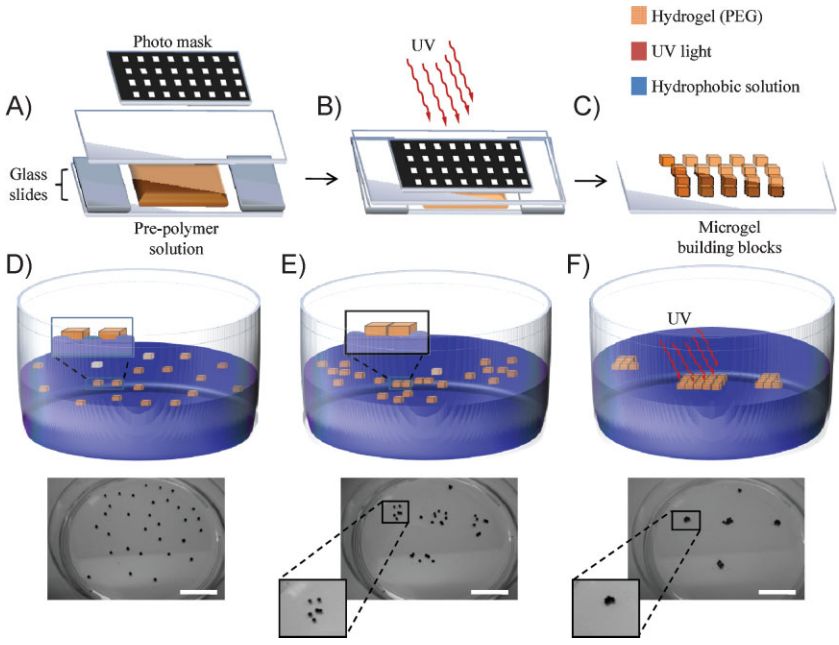

Figure 1. Schematic illustration of the liquid–air-interface-directed self-assembly technique. A) A PEG–cell solution is placed on top of an OTS-treated glass slide between the photomask and spacers. B) UV light is selectively filtered through the photomask, causing the PEG–cell solution to polymerize in the desired pattern. C) Following washing with PBS, all that remains are cell-laden PEG microgels of the desired geometry. D) Microgels are randomly placed on the surface of either PFDC or CCl_4, where they remain due to the high density of the solutions. E) Due to surface tension, the particles self-assemble to minimize free energy. F) Secondary UV polymerization crosslinks the microgels to each other, leading to macroscale engineered microgels. Scale bar is 2 cm.

NANO MICRO small

surface of carbon tetrachloride (CCl_4) or perfluorodecalin (PFDC) (Figure 1D) to fabricate 3D tissue-like constructs. PFDC and CCl_4 were chosen from a list of potential solutions because they are denser than water, thus ensuring that the microgel blocks would float, and because of their hydrophobicity, which kept the hydrogel blocks on the surface and helped induce aggregation.[6,16] However, only PFDC was used in cell-laden assembly experiments due to the excessive toxicity caused by CCl_4 exposure.[17] Due to the surface tension on the liquid–air interface, the hydrogels moved towards each other and began aggregating to minimize the system free energy (Figure 1E). Since the hydrogels were bound only through minimization of the surface free energy, a secondary crosslinking step was used to stabilize the microgel assemblies and create centimeter-scale tissue structures (Figure 1F). It is not necessary to add additional unreacted PEG to be able to achieve secondary and tertiary polymerizations, consistent with previous studies.[7] This technique, which exposed the gel blocks to UV light for a short time, successfully formed tightly packed, centimeter-scale 3D tissue sheets consisting of multiple microgel subunits with square, triangular, and hexagonal geometries (Figure 2). While this technique could be used with a wide variety of microgel shapes, the optimum microgel geometry for cell and tissue function may not always correlate with optimum aggregation. The resulting cell sheets could potentially be used for tissue engineering applications of vascular,[18] corneal, bladder, and other tissues with the added benefit of controlling the cellular microenvironment in 3D.

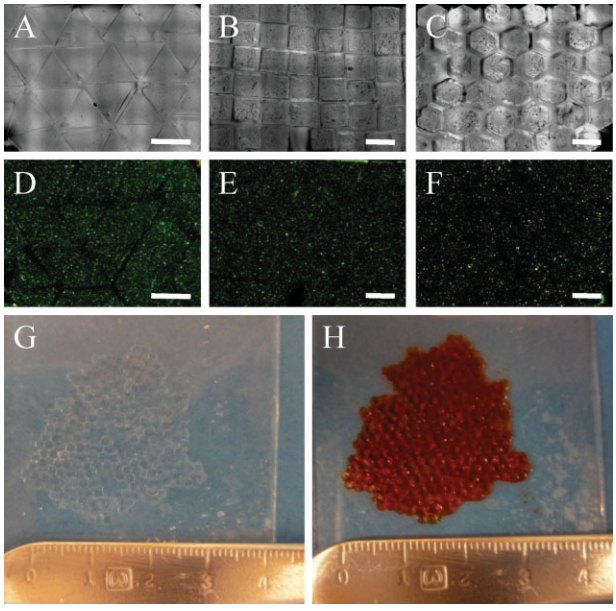

Figure 2. Histological images of centimeter-scale engineered gel sheets created by the interface-directed assembly of microgel blocks. A) Triangular, B) square, and C) hexagonal building blocks were assembled on the surface of either CCl_4 or PFDC and secondarily crosslinked to form engineered gel sheets. D–F) Live/dead staining demonstrated a high level of cell viability in all cases. G) Formation of macroscale structures with overall dimensions on the centimeter scale made from hexagonal microgels. H) To improve visualization, the microgels were labeled with a red food-coloring dye. Scale bar is 1 mm.

Previously, self-assembly has shown great potential, yet with inherent limitations for various applications such as tissue engineering. For example, Whitesides and coworkers developed approaches to assemble mesoscale structures with similar conceptual elements to the present work.[6,16] Their work demonstrated the utility of the self-assembly of polydimethylsiloxane (PDMS) modules on the surface of PFDC. Improved control over the assembly process was implemented by rendering certain faces of the modules hydrophobic or hydrophilic. However, PDMS modules were unable to bind following aggregation, limiting their utility when not on the solution surface and making removal of the assembled structures difficult. In contrast, by using hydrogels, our system was able to use cell-laden modules for creating engineered tissues. In a previous report, we demonstrated the self-assembly of cell-laden PEG microgels within hydrophobic mineral oil to create higher-order structures.[7] Drawbacks of the previous technique include the limited control over the resulting sizes of the assembled structures, which were in the micrometer-scale range, as well as limitations on the efficiency of the assembly process. Assembling cell-laden microgels on a dense hydrophobic surface allows for much greater overall structure sizes on the centimeter scale. The current technique also offers greater control over the directed assembly process at the micro- and macro-scales than previous techniques, which employed random assembly only within defined containment structures, such as perfusion tubing[19] or cells seeded onto structures following creation.[8,9]

2.2 Cell Viability

To assess the effects of UV exposure and the assembly process on cell viability, samples were collected following each step of the procedure and analyzed using a live/dead assay (Figure 3). Cell viability was determined for cells mixed in the prepolymer solution, following 27 s UV exposure leading to polymerized microgels (Figure 3A–B), after 1-min exposure of cell-laden microgels to the surface of PFDC (Figure 3C), and following secondary UV exposure for 5 s, leading to 3D tissue formation in PFDC (Figure 3D). Cell-laden microgels were then cultured statically in basal media with viability determined on days 1, 3, 5, and 7 (Figure 3E–H), while quantification of viability was performed for 5 samples for each condition (Figure 3I). The live/dead analysis demonstrates that viability remained above 90% following UV and PFDC exposure, demonstrating that neither significantly affected cell viability. In summary, throughout the fabrication and assembly processes, cell viability remained virtually unchanged. Cell viability was then tracked over a one-week period to assess the feasibility of the current assembly technique for creating long-term engineered tissues. Viability remained above 90% on days 1 and 3 and remained at or above 85% for up to one week. There were no significant losses in viability throughout the process or subsequent culture, demonstrating the suitability of this technique for creating robust long-term tissue-like structures. As UV and PFDC exposure has been demonstrated to show no significant effect on short-term or long-term cell viability, we believe that using UV to bind multiple microgel sheets together to form 3D tissue structures

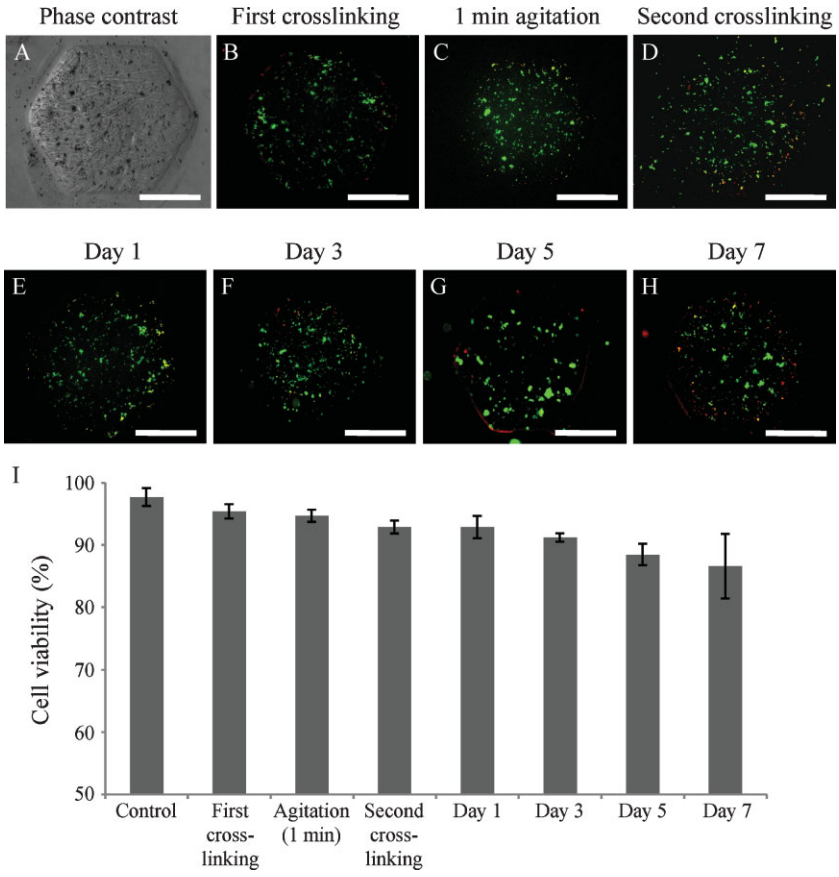

Figure 3. Cell-viability analysis as a function of steps in the assembly procedure. A) Hexagonal cell-laden hydrogels were created and the viability was tracked following exposure to UV light and PFDC. B) PEG–cell mixtures were polymerized by UV exposure and placed on the surface of PFDC, C) stirred for 1 min in PFDC, and D) secondarily crosslinked with UV light. Cell-laden microgels were then cultured for E) 1, F) 3, G) 5, and H) 7 d in cell-culture medium. I) Quantification of samples ($n = 5$) at each timepoint demonstrated that viability did not significantly decrease due to UV or PFDC exposure or time in culture. Scale bar is 500 μm.

would not maintain high cell viability. In addition, provided that the exposure times remain on the order presented, increasing the number of UV and PFDC exposures to create more intricate microgel assemblies should not significantly alter either the short- or long-term viability in assembled structures.

2.3 Theoretical Rationale

Solid particles floating on the surface of a dense liquid can deform the liquid surface, thereby generating lateral capillary forces, which may be repulsive or attractive depending on the particle weight, geometry, and wetting properties.[20–22] The capillary forces move the floating particles so as to reduce the total free surface area and the system energy. By tuning the mass and the geometrical and wetting properties, the particles can self-assemble into various patterns.[6,23,24] In general, it has been found experimentally and theoretically that particles aggregate based on the simple rule ''like menisci attract, unlike menisci repel''. Since our system is composed of identical particles, these will attract. The degree of attraction, and hence the speed of aggregation, depends on the wetting and geometrical properties of the particular solid-particle–liquid combination. The capillary forces extend over a length scale $l_c = \sqrt{\gamma/\rho g}$, the capillary length, where γ is the surface tension of the gas/fluid interface, ρ is the fluid density, and g is the acceleration due to gravity. For CCl_4 at 25°C,[25,26] $\rho = 1.58\,\mathrm{g\,mL^{-1}}$, $\gamma = 26.1\,\mathrm{dynes\,cm^{-1}}$, and $l_c = 1.3\,\mathrm{mm}$; for PFDC,[27,28] $\rho = 1.93\,\mathrm{g\,mL^{-1}}$, $\gamma = 19.4\,\mathrm{dynes\,cm^{-1}}$, and $l_c = 1.0\,\mathrm{mm}$. The relative importance of gravity and surface tension is quantified by the (dimensionless) Bond number, $B_0 = (d/l_c)^2$, where d is the particle diameter. In our system, $d \approx 200$–$1000\,\mu\mathrm{m}$ and B_0 is 0.024–0.60 for CCl_4 and 0.039–0.98 for PFDC. Hence, for the smaller sizes, capillary forces dominate gravity and particles rely primarily on their geometry and wetting properties, and not their weight, to deform the free surface and experience the concomitant capillary forces. Capillary attraction between light particles dominates thermal energy for particle sizes down to the nanometer scale.[15,29] Lastly, since viscous drag and the capillary force on a particle both scale with its diameter, these forces scale down proportionally. Thus, the capillary-force-driven self-assembly observed in our model system is scalable to the nanometer scale.

Theoretical approaches could be used to tune the particle design and wetting properties to optimize the self-assembly process in our system. The static free surface is described by the Young–Laplace equation, which admits analytic solutions for simple geometries such as the free surface between parallel infinite walls or cylinders.[30,31] For more complex geometries like spherical, square, triangular, and hexagonal bodies, the free surface must be computed numerically, though approximate formulas exist for small surface slopes and large particle spacing.[15,20,32–35]

2.4 Aggregation Factor and Parameter Optimization

To fabricate tissue-like constructs with physiologically relevant cell densities, geometries, and microarchitectures, it is essential to maximize the microgel packing by optimizing the microgel aggregation. To achieve this goal, several parameters were optimized, such as the molecular weight of PEG, microgel dimensions, and the number of microgels in the hydrophobic solution. To evaluate the parameter optimization, an aggregation factor (A_f) was defined as follows:

$$A_f = 1 - \frac{a_f}{n \times a_i} \quad (1)$$

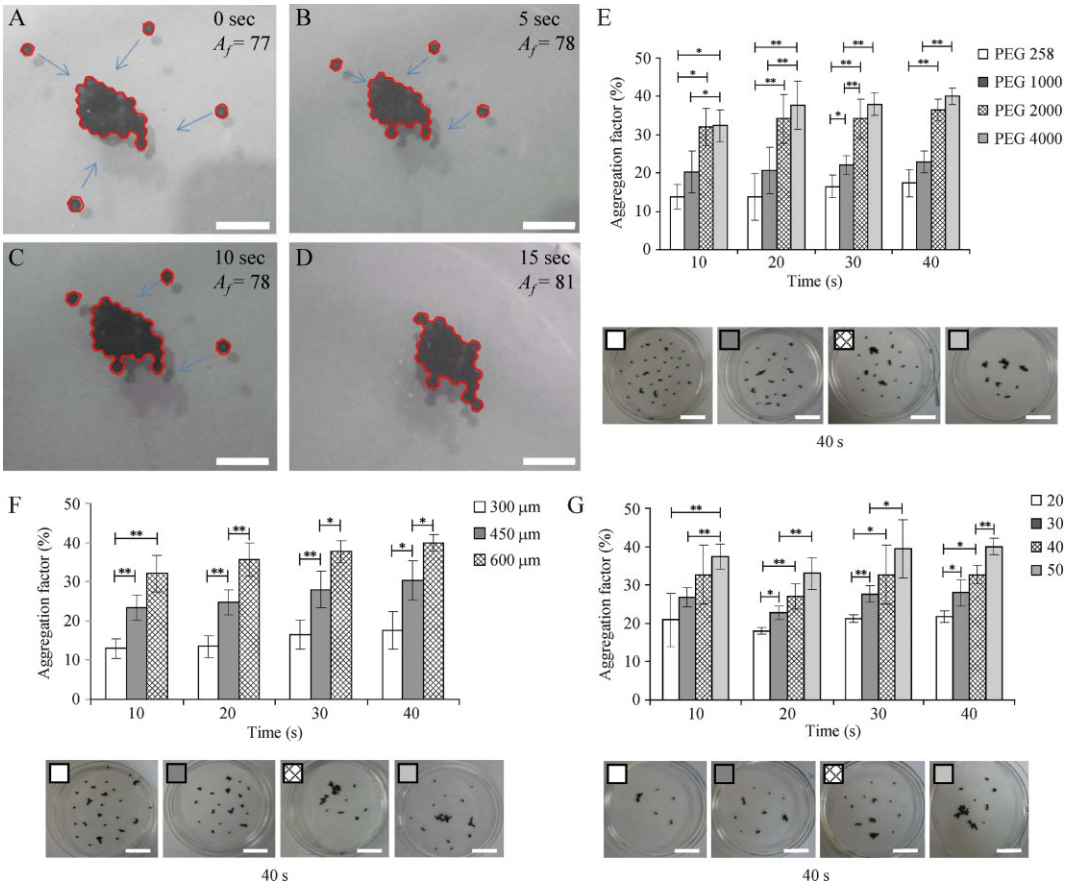

Figure 4. Optimization of microgel assembly. A–D) The assembly process was tracked in 5 s intervals to demonstrate how the aggregation factor (A_f) changed with time. A_f was increased by E) increasing the molecular weight of PEG from 258 to 2000 Da, F) increasing the thickness of the microgels from 300 to 600 μm, and G) increasing the number of microgels on the solution surface. F) No further improvements were found by using PEG with a molecular weight of 4000 Da. Scale bars are 10 mm (A–D) and 2 cm (E–G). Statistical significances of $p < 0.05$ and $p < 0.01$ are represented by * and **, respectively.

where a_f is the sum of the areas of the microgel faces in contact with the interface (i.e., the contact line), a_i is the sum of the areas of the faces of one microgel in contact with the interface, and n is the total number of microgels. In the case where there is no aggregation $a_f/(na_i) = 1$ and $A_f = 0$. Figure 4A–D illustrates the gradual increase of the aggregation factor as the microgels aggregate. The red line shows the contact line where the interface meets the aggregated structure. Once microgels join the aggregated structure, a_f decreases and, since a_i is constant for a specific microgel block, the aggregation factor A_f rises.

The evolution of the aggregation factor is shown in Figure 4 and demonstrates that the aggregation factor increased with time and molecular weight. As time passed, the surface tension had more time to aggregate the microgel blocks. Increasing the molecular weight of PEG improved the aggregation by increasing the hydrophilicity of the microgels, thereby increasing the difference in the initial and final free energy of the system (Figure 4A–D). Increasing the molecular weight of PEG from 258 to 4000 Da resulted in a roughly three-fold increase in the aggregation factor from 12 to 35% (Figure 4E, $p < 0.05$). Similarly, increasing the thickness of the microgels from 300 to 600 μm more than tripled the aggregation factor from 10 to 33% (Figure 4F, $p < 0.05$). Also, increasing the number of initial building blocks from 20 to 50 increased the aggregation factor from 26 to 36% (Figure 4G, $p < 0.05$).

2.5 Effects of Agitation on Aggregation

To increase the packing density of the resulting macrostructures and to increase the speed and completeness of aggregation, centripetal forces were applied to the system by means of stirring. Stirring improves the aggregation by creating a depression on the free surface, which allows gravity to help drive the particles toward each other. We investigated two hydrophobic solutions, PFDC and CCl_4, each with four different rotational speeds (Figure 5). Stirring at a rate of 200 rpm increased the aggregation factor from 34% (no stirring) to 80% for CCl_4 ($p < 0.05$). Similar behavior was observed for PFDC when the rotational speed was increased from 0 to 200 rpm, increasing A_f from 24 to 82%, respectively ($p < 0.05$). Furthermore, increasing the stirring speed to 300 rpm significantly decreased the aggregation factor from

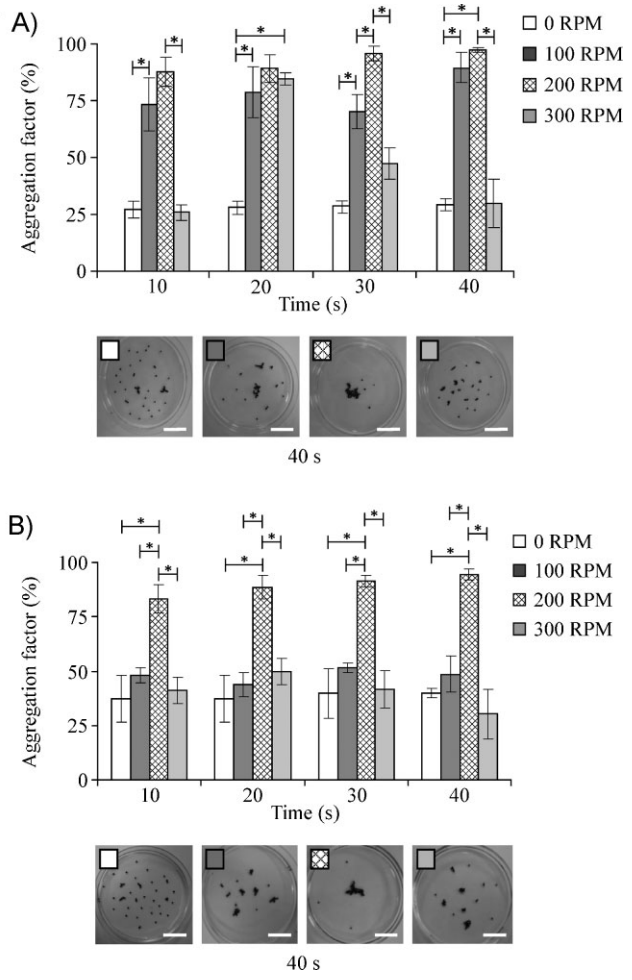

Figure 5. Effects of stirring speed on interface-directed microgel assembly. A) Stirring at a speed of 100 or 200 rpm caused a significantly higher A_f than no stirring ($p < 0.05$) or a stirring rate of 300 rpm ($p < 0.05$) on the surface of PFDC. B) Generally similar behavior was seen for interface-directed assembly on the surface of CCl_4. However, only a stirring speed of 200 rpm significantly improved A_f, while stirring rates of 100 or 300 rpm showed no improvement over static culture ($p < 0.05$). Inset: representative images of assembly following 40 s agitation at each speed for PFDC and CCl_4. Scale bar is 2 cm. Statistical significance of $p < 0.05$ is represented by *.

80 to 36% for CCl_4 and 82 to 36% for PFDC ($p < 0.05$). The optimized stirring speeds determined here depended on the solution volume and depth, and are therefore only valid for the conditions described.

While larger aggregate sizes were not attempted in this study, there should not be any physical limit to the overall structure size achievable using this technique. Given the availability of dishes with sufficiently large diameters, sufficient quantity of PFDC, and a large coverage area for the UV exposure (or multiple exposures covering smaller individual areas), any desired size could seemingly be constructed. In addition, while the overall structure shape tended to be circular, asymmetrically shaped dishes, such as squares or rectangles, could allow for more control over the shape of the assembly. However, this would likely also decrease the efficiency of aggregation as the stirring would not be applied equally to all regions. Another method for producing shaped assemblies would be to create circular sheets and to cut them to shape. Though not optimally efficient, this method could rapidly produce controlled structure sizes and shapes since tens to hundreds of microgels can be created with 1 UV step and aggregated into sheets in minutes.

2.6 Spatial Control of Cell Seeding in Engineered Tissue Constructs

Fabricating complex tissues requires the coculture of different cell types in physiologically relevant geometrical patterns. However, a limitation of many fabrication techniques is the lack of spatial control of specific cell types within engineered tissues. In this report, multiple cell-laden microgels of identical shapes and dimensions were rapidly aggregated and polymerized into robust, 3D tissue-like constructs. While this approach facilitated the rapid formation of tissue constructs, the microgel assembly was governed primarily by random interactions. Therefore, this technique could be used to create tissue layers with microgels of multiple cell types but could not spatially control the cocultured cell-laden microgels. To address this issue a hierarchical approach was developed to facilitate spatial control over cell placement in the engineered tissues.

In the hierarchical approach, the tissue of interest is constructed through a multistep process. Individual microgels of similar shapes, each containing one cell type, were created as described previously, using either rhodamine- or fluorescein isothiocyanate (FITC)-labeled cells. Next, one hydrogel with rhodamine-labeled cells was placed on the hydrophobic solution surface, loosely surrounded by six hydrogels of the same structure with FITC-labeled cells. The FITC-labeled microgels aggregated to form a fully packed structure surrounding the rhodamine-labeled microgel. These fabricated structures were photocrosslinked and then used as building blocks for a subsequent assembly process to create centimeter-scale, tightly packed tissues with spatially controlled coculture. Figure 6A shows a schematic representation of this process. Figure 6B and C shows phase-contrast and fluorescent images of the resulting structure, respectively. To enact even further control over the coculture and overall assembly parameters, lock-and-key structures were employed, further demonstrating the versatility of this technique (Figure 6D–F).

While the creation of these complex, coculture building blocks was more time consuming than with singular microgel building blocks, the hierarchical technique allowed for precise control over the coculture cell distribution, while being compatible with the high-throughput production of large tissue-like sheets. Moreover, each complex building block was created in under one minute. These complex blocks could be produced in parallel and then rapidly assembled using a high-throughput approach, making the overall technique still relatively rapid. One negative aspect of this multistep approach was a reduced yield in complex building blocks, which was balanced by the improved level of spatial

NANO MICRO small

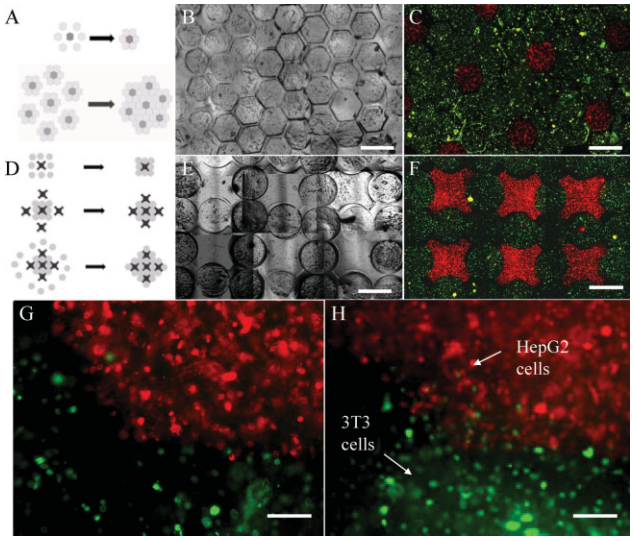

Figure 6. Creation of interface-directed microgel structures with controlled coculture. A) A cartoon representation of the assembly of complex building blocks using a central microgel with one cell type (dark gray) surrounded by building blocks of a second cell type (light gray) on the surface of PFDC or CCl_4. The complex building blocks consisting of 7 hexagonal microgels could then be used for interface-directed assembly into tissue-like structures with spatially controlled coculture conditions. B) Phase-contrast and C) fluorescence images of engineered centimeter-scale tissues using complex building blocks with controlled coculture conditions. D) A schematic representation of the assembly of complex building blocks with controlled coculture using lock-and-key-shaped microgels to better direct the assembly process. E) Phase-contrast and F) fluorescence images of engineered centimeter-scale tissues using lock-and-key complex building blocks with controlled coculture conditions. Scale bar is 1 mm. The coculture of 3T3 and HepG2 cells using the assembly process shown in (A), having blocks with encapsulated HepG2 cells surrounded by six blocks with encapsulated 3T3 cells after G) 1 and H) 7 d. Scale bar is 100 μm.

control of cell deposition within the tissue-like constructs. The hierarchical technique combines many of the positive spatial cell-seeding aspects of previous techniques like sequential photopolymerization or organ printing,[36,37] but without the need for specialized equipment or technical expertise, greatly increasing the possible applications and potential users.

In addition, we incorporated cell-responsive photocrosslinkable hydrogels with our assembly technique. Using gelatin methacrylate (GelMA), we demonstrated that cocultured cells could migrate across microgel borders to interact with neighboring cells (Figure 6G–H). The migration could be more precisely controlled through the creation of very specific cell binding and degradation sites using PEG as described previously.[38,39] One potential drawback to the technique presented is the necessity that any desired hydrogel be polymerized through photocrosslinking, limiting the pool of available materials. However, as the data demonstrate, diminished viability due to UV exposure is not a major concern. In addition, UV crosslinking rapidly polymerizes the microgels (in seconds), avoiding the gravitational settling of cells and ensuring an even 3D cell distribution. Other polymerization techniques are not as rapid.

3. Conclusions

This work introduces a fabrication method for creating cell-laden tissue-like structures using a bottom-up self-assembly approach in a multiphase environment (liquid–air system). This technique can be used to rapidly create tightly packed tissue-like sheets with either single cell types or homogeneously distributed coculture. In addition, a hierarchical approach was demonstrated that can create complex multigel building blocks with precisely controlled coculture distribution to create tissue-like constructs with specific cell distribution. Even greater control over this technique can be achieved by using specific structures, such as lock-and-key assemblies, to better direct the assembly of cocultured tissues. The ability to precisely control the cell distribution within self-assembled tissue-like constructs could greatly improve engineered tissue function and morphology. This technique could create single-layer implants or could be combined with existing cell-sheet techniques to create multilayer engineered tissues, providing more control than is currently possible with traditional cell-sheet techniques. Future work will expand the directed-assembly technique to include more than two cell types, multiple shapes, and more intricate lock-and-key assemblies, enabling advances in the field of engineered tissues with controlled cell distribution and microarchitectural features.

4. Experimental Section

Preparation of microgels: Microgels were prepared by dissolving 20 w/w% PEG (4000 Da, Monomer-Polymer & Dajac Labs, Inc.) in Dulbecco's phosphate-buffered saline (DPBS, GIBCO). The hydrogel units were fabricated through UV polymerization on the surface of a glass slide. To ease the detachment of the hydrogel from the glass surface following polymerization, glass slides were treated with ocadecyltrichlorosilane (OTS, Sigma) as previously described.[7] Before UV polymerization, 1 w/w% photoinitiator 2-hydroxy-1-(4(hydroxyethoxy) phenyl)-2methyl-1propanone (Irgacure 2959, CIBA Chemicals) was added to the prepolymer solution. Photomasks, with different patterns and sizes (dimensions in μm: 200 × 200, 400 × 400, 600 × 600, 800 × 800, and 1000 × 1000) were designed in AutoCAD and printed on transparencies at a resolution of 20 000 dpi (CAD/Art Services). Different basic shapes (square, triangular, and hexagonal) were used to demonstrate the assembly technique's versatility and its utility for recreating a wide variety of native tissue units. The photomasks were placed on a cover slip between the UV light source and prepolymer solution to selectively expose the polymer to the light. A droplet containing 35 μL of the photocrosslinkable PEG prepolymer was placed on a glass slide covered by a cover slip separated by different numbers of spacers (cover slips, thickness = 150 μm) to provide hydrogel units with controlled thicknesses. UV light (360–480 nm; 12.4 mW cm^{-2}) was passed through the photomask for 27 s to polymerize the PEG in the desired microgel shapes. The entire self-assembly procedure is illustrated in Figure 1.

Following UV polymerization, the building blocks were carefully detached from the OTS-treated glass slide and randomly

placed on the surface of dense, hydrophobic solutions (60 mL) that were made of PFDC or CCl_4 (Aldrich) in a standard $100 \times 15\ mm^2$ Pyrex reusable Petri dish (Fisher Scientific). To quantify the degree of assembly, the aggregation factor was calculated as defined above. To enhance the aggregation of microgels, stirring was applied to the system with different speeds using a Corning stirrer (PC-620D, Preiser Scientific). To create tissues from the aggregated, cell-laden microgels, following interface-directed self-assembly, the final product was exposed to UV for an additional 5 s. Microgels were then washed five times with PBS following PFDC exposure to remove excess PFDC and improve cell viability. In certain cases, to distinguish the microgels, the prepolymers were mixed with rhodamine–dextran ($M_r = 10$ kDa) or fluorescent FITC microbeads (1%, 5-μm diameter, Duke Scientific) at a concentration of 0.3 mM prior to the initial UV exposure.

Fabrication of cell-laden microgel assemblies: Fibroblast cells (NIH-3T3) were cultured in Dulbecco's modified Eagle's medium (DMEM) supplemented with 10% fetal bovine serum (FBS; GIBCO) in a 5%-CO_2-humidified incubator at 37 °C. To harvest and encapsulate cells, the cells were first trypsinized with 1% trypsin (GIBCO) and centrifuged at 1000 rpm for 5 min. The harvested cells were mixed with PEG prepolymer at a concentration of 1×10^7 cells mL^{-1}. Cell-laden PEG was used in a similar manner to cell-free PEG to create microgels, as described above. To generate a 3D model of cocultures of different cell types, cells were separated into two groups and labeled with either Calcein AM (green) or PKH26 (red) fluorescent cell tracker (Sigma). In addition, cocultured assemblies were performed in 5 w/v% GelMA instead of PEG since GelMA has similar behavior to PEG but allows cell elongation and migration.[29] To investigate cell viability at each stage, select unlabeled cell-laden microgels were analyzed using a live/dead assay according to the manufacturer's instructions (Molecular Probes).

Statistical evaluation: Data were expressed as mean ± standard deviation (SD). Differences between groups were analyzed using Student's one-tailed t test with p values less than 0.05 considered significant. The group size was $n = 5$ for all groups analyzed in the parameter-optimization part and was $n = 3$ for the cell-viability tests. $p < 0.05$ is represented by a single star and $p < 0.01$ is represented by a double star in the graphs. All error bars present the SD.

Acknowledgements

This work was supported by the National Institutes of Health (EB007249; DE019024; HL092836), the NSF CAREER award, the Institute for Soldier Nanotechnology, and the US Army Corps of Engineers. We would like to thank Dr. Yanan Du, Dr. Seunghwan Lee, Dr. Won Gu Lee, and Dr. Jalil Mostashari for their scientific and technical support.

[1] R. Langer, J. P. Vacanti, *Science* **1993**, *260*, 920–926.
[2] A. Khademhosseini, J. P. Vacanti, R. Langer, *Sci. Am.* **2009**, *300*, 64–71.
[3] N. L'Heureux, T. N. McAllister, L. M. de la Fuente, *New Engl. J. Med.* **2007**, *357*, 1451–1453.
[4] A. Khademhosseini, R. Langer, J. Borenstein, J. P. Vacanti, *Proc. Natl. Acad. Sci. USA* **2006**, *103*, 2480–2487.
[5] L. Costanzo, *Physiology*, Lippincott, Williams & Wilkins, Philadelphia **2006**.
[6] G. M. Whitesides, B. Grzybowski, *Science* **2002**, *295*, 2418–2421.
[7] Y. Du, E. Lo, S. Ali, A. Khademhosseini, *Proc. Natl. Acad. Sci. USA* **2008**, *105*, 9522–9527.
[8] D. M. Dean, A. P. Napolitano, J. Youssef, J. R. Morgan, *FASEB J.* **2007**, *21*, 4005–4012.
[9] A. P. Napolitano, P. Chai, D. M. Dean, J. R. Morgan, *Tissue Eng.* **2007**, *13*, 2087–2094.
[10] G. M. Hoben, J. C. Hu, R. A. James, K. A. Athanasiou, *Tissue Eng.* **2007**, *13*, 939–946.
[11] A. P. McGuigan, M. V. Sefton, *Proc. Natl. Acad. Sci. USA* **2006**, *103*, 11461–11466.
[12] N. Peppas, J. Z. Hilt, A. Khademhosseini, R. Langer, *Adv. Mater.* **2006**, *18*, 1–17.
[13] J. W. Nichol, A. Khademhosseini, *Soft Matter* **2009**, *5*, 1312–1319.
[14] A. Khademhosseini, R. Langer, *Biomaterials* **2007**, *28*, 5087–5092.
[15] P. A. Kralchevasky, K. Nagayama, *Adv. Colloid Interface Sci.* **2000**, *85*, 145–192.
[16] N. Bowden, A. Terfort, J. Carbeck, G. M. Whitesides, *Science* **1997**, *276*, 233–235.
[17] F. Malchiodi-Albedi, R. Perilli, G. Formisano, G. Scorcia, S. Caiazza, *J. Biomed. Mater. Res.* **1998**, *41*, 608–613.
[18] N. L'Heureux, N. Dusserre, G. Konig, B. Victor, P. Keire, T. N. Wight, N. A. Chronos, A. E. Kyles, C. R. Gregory, G. Hoyt, R. C. Robbins, T. N. McAllister, *Nat. Med.* **2006**, *12*, 361–365.
[19] A. P. McGuigan, D. A. Bruzewicz, A. Glavan, M. Butte, G. M. Whitesides, *PLoS ONE* **2008**, *3*, 1–11.
[20] C. Allain, M. Cloitre, *J. Colloid Interface Sci.* **1993**, *157*, 261–268.
[21] B. A. Grzybowski, N. Bowden, F. Arias, H. Yang, G. M. Whitesides, *J. Phys. Chem. B* **2001**, *105*, 404–412.
[22] E. H. Mansfield, H. R. Sepangi, E. A. Eastwood, *Philos. Trans. R. Soc. A* **1997**, 869–919.
[23] D. B. Wolfe, A. Snead, C. Mao, N. B. Bowden, G. M. Whitesides, *Langmuir* **2003**, *19*, 2206–2214.
[24] G. M. Whitesides, M. Boncheva, *Proc. Natl. Acad. Sci. USA* **2002**, *99*, 4769–4774.
[25] Q. H. Nguyen, A. B. Ponter, W. Peier, *J. Chem. Eng. Data* **2002**, *23*, 54.
[26] V. T. Lam, G. C. Benson, *Can. J. Chem.* **1970**, *48*, 3773–3781.
[27] A. M. A. Dias, C. M. B. Goncalves, A. I. Caco, L. Santos, M. M. Pineiro, L. F. Vega, J. A. P. Coutinho, I. M. Marrucho, *J. Chem. Eng. Data* **2005**, *50*, 1328–1333.
[28] M. G. Freire, P. J. Carvalho, A. J. Queimada, I. M. Marrucho, J. A. P. Coutinho, *J. Chem. Eng. Data* **2006**, *51*, 1820–1824.
[29] J. A. Benton, C. A. Deforest, V. Vivekanandan, K. S. Anseth, *Tissue. Eng. A.* **2009**, *15*, 3221–3230.
[30] H. Lamb, *Statics, including Hydrostatics and the Elements of the Theory of Elasticity*, Cambridge University Press, Cambridge, UK **1912**.
[31] M. A. Fortes, *Can. J. Chem.* **1982**, *60*, 2889–2895.
[32] H. Shinto, D. Komiyama, K. Higashitani, *Langmuir* **2006**, *22*, 2058–2064.
[33] P. Singh, D. D. Joseph, *J. Fluid Mech.* **2005**, *530*, 31–80.
[34] M. M. Nicolson, *Proc. Camb. Philos. Soc.* **1949**, *45*, 288–295.
[35] W. A. Gifford, L. E. Scriven, *Chem. Eng. Sci* **1971**, *26*, 287–297.
[36] N. E. Federovich, J. R. DeWijn, A. J. Verbout, J. Alblas, W. J. A. Dhert, *Tissue Eng. A* **2008**, *14*, 127–133.
[37] E. A. Roth, T. Xu, M. Das, C. Gregory, J. J. Hickman, T. Boland, *Biomaterials* **2004**, *25*, 3707–3715.
[38] B. K. Mann, A. S. Gobin, A. T. Tsai, R. H. Schmedlen, J. L. West, *Biomaterials* **2001**, *22*, 3045–3051.
[39] A. S. Gobin, J. L. West, *FASEB J.* **2002**, *16*, 751–753.

Received: December 14, 2009
Published online: March 31, 2010

